Geological Magazine

www.cambridge.org/geo

Original Article

Cite this article: Kumar M, Prakash D, Singh CK, Yadav MK, Tewari S, Singh PK, and Mahanta B (2023) Geochronology and oxygen fugacity of the pelitic granulite from the Diwani hills, NE Gujarat (NW India). *Geological Magazine* **160**: 22–34. https://doi.org/10.1017/S0016756822000607

Received: 22 December 2021
Accepted: 26 May 2022
First published online: 1 August 2022

Keywords:
Aravalli–Delhi Mobile Belt; Perple_X; Neoproterozoic; oxygen fugacity; granulites

Author for correspondence: D. Prakash, Email: dprakash_ynu@yahoo.com

Geochronology and oxygen fugacity of the pelitic granulite from the Diwani hills, NE Gujarat (NW India)

Manish Kumar[1], D. Prakash[1], C. K. Singh[1], M. K. Yadav[2], S. Tewari[3], Pradip K. Singh[1] and B. Mahanta[1]

[1]Centre of Advanced Study in Geology, Banaras Hindu University, Varanasi, 221005, India; [2]Centre of Advanced Study in Geology, University of Lucknow, Lucknow, 226007, India and [3]School of Environmental and Earth Sciences, Central University of Punjab, Bathinda, India

Abstract

The Diwani hills are located SE of Balaram–Abu Road in the Banaskantha district of north Gujarat. The crystalline rocks of the Diwani hill area are a diverse assemblage of Precambrian metamorphic and igneous rocks. These rocks are petrologically more complex and date back to the Aravallis or earlier. The mineralogical assemblages such as grt–sp–opx–qz of these rocks indicate their origin in anhydrous or dry conditions, implying metamorphism under pyroxene granulite facies. These granulitic rocks were subjected to Delhi orogenic deformation and were later intruded by the Erinpura granite. Textural and microstructural relationships, mineral chemistry, *P*–*T*–*X* pseudosection modelling and the oxidation state of pelitic granulites from the Diwani hill area of north Gujarat are all part of the current approach. The winTWQ program and pseudosection modelling in the NCKFMASHTO model system utilizing Perple_X software were used to restrict the *P*–*T* evolution of these pelitic granulites. The unification of these estimates shows that the pelitic granulites reached their pressure and temperature maxima at 8.6 kbar and 770 °C, respectively. The oxygen fugacity (log fO_2) versus temperature computations at 6.2 kbar revealed log fO_2–*T* values of −13.0 and 765 °C, respectively. The electron microprobe dating of monazite grains separated from the granulites of the Diwani hills yields ages ranging from 769 Ma to 855 Ma. The electron microprobe dating presented here from the Diwani hills provides evidence for a Neoproterozoic (Tonian) metamorphic event in the Aravalli–Delhi Mobile Belt.

1. Introduction

The major Palaeoproterozoic orogenic mobile belts in India surrounding Archaean cratons extend from the northwest to the east through the central part of the Indian peninsula. They preserve a broad history of metamorphism, magmatism and sedimentation (Naqvi & Rogers, 1987; Valdiya, 2010). The Diwani hill granulites lie in the southern part of the Aravalli–Delhi Mobile Belt, which is an important crustal feature in the northwestern part of India and preserves a polyphase deformational history (Prakash *et al.* 2021). Textural (textural relationships between minerals and zoning patterns) and structural studies of the rocks from such an orogenic belt that has suffered multiple phases of tectonic disturbances would aid in delineating the *P*–*T*–*t*–*d* path it has travelled in the due course of its evolutionary phases (Triboulet & Audren, 1985; Schulz, 1990; Cho *et al.* 2007; St-Onge *et al.* 2013; Gomez-Rivas *et al.* 2020; D'Souza *et al.* 2021).

The Balaram–Abu Road area is situated in the northern part of Gujarat state and extends to some southern parts of Rajasthan state, India. Petrologically, the entire landscape around the Balaram area (Fig. 1) consists of granulite-facies metamorphic rocks deformed during the Delhi orogeny and, later, intruded by the Erinpura granite (Srikarni *et al.* 2004; Singh *et al.* 2010; Prakash *et al.* 2021). The occurrence of granulite-facies rocks in the Balaram–Abu Road area was first reported by Desai *et al.* (1978). Charnockites, norites–metanorites, pelitic granulites, calc-granulite, granite gneiss and granite are the most common rock types in the Balaram–Abu Road area (Desai *et al.* 1978). Pelitic granulites in the area show gneissic structures and are composed of minerals such as spinel, cordierite, garnet, sillimanite, hypersthene, feldspar, quartz, biotite and plagioclase segregated in the coarse dark- and light-coloured bands. The dark bands are predominantly rich in cordierite with reddish brown garnets strewn throughout, while the light bands are composed of quartzo-feldspathic material (Prakash *et al.* 2021).

These granulites provide information related to the chemical, petrological and tectonic evolution of the Earth's middle and lower crust (Singh *et al.* 2010; Prakash *et al.* 2021). Therefore, they play a crucial role in understanding the crustal petrogenesis as well as tectonometamorphic evolution of a region. Fluid and redox potential (oxidation state) play essential roles in the

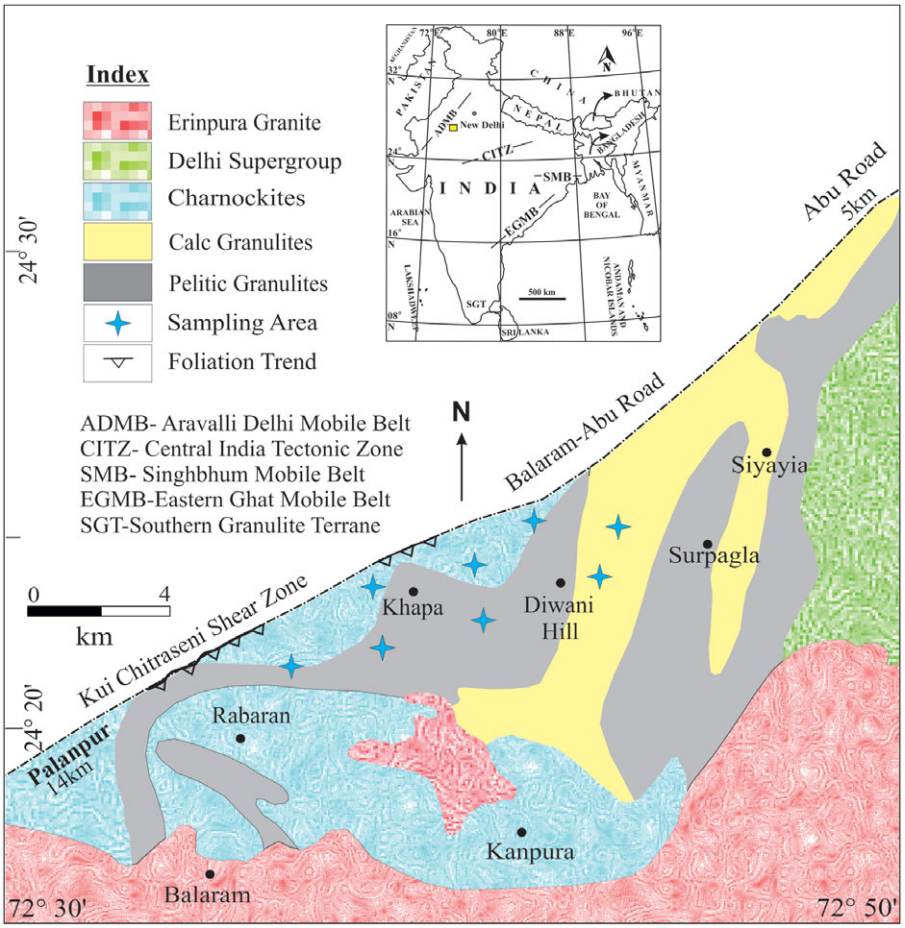

Fig. 1. (Colour online) Map showing different tectonic elements and sample location of the study area (map modified after Prakash *et al.* 2021).

recrystallization and development of mineral phases during granulite-facies metamorphism. Except for a few preliminary works, no significant effort had been made previously in the area to understand the role of fluid activity and oxidation conditions during the granulite-facies metamorphism in the Diwani hills. In the present work, an attempt has been made to quantify the oxidation conditions and carry out pseudosection modelling and monazite dating to understand the tectonometamorphic evolution of the Diwani hill area of the Aravalli–Delhi Mobile Belt. The current approach encompasses study of textural and microstructural relationships, mineral chemistry, *P–T–X* pseudosection modelling, oxidation state and geochronology of the pelitic granulites from the Diwani hill area.

2. Geological outline of the study area

The Aravalli–Delhi Mobile Belt is a vital crustal morphotectonic unit of northwestern India which represents ~3.2 Ga (Roy & Kröner, 1996) and trends in a NE–SW direction (Hazarika *et al.* 2013). The oldest rock unit of the craton (Mewar) is represented by a Meso- to Neoarchaean Banded Gneissic Complex (BGC), which may easily be found exposed in the central and southern parts of the terrane as granulite- to amphibolite-facies orthogneisses and/or supracrustal metasediments (Gupta, 1934; Heron, 1953; Mahadani *et al.* 2015). The entire BGC may be further classified into two parts as BGC I and BGC II. Multiple episodes of Neoarchaean granitic emplacement, viz. the Untala, Gingla, Berach, Ahar River, Jahazpur and Malola granites, occurred within the rocks of the BGC (D'Souza *et al.* 2019). Based on the metamorphic ages and rock types, Sinha-Roy *et al.* (1995) reclassified the BGC II into two parts: the Sandmata complex and the Mangalwar complex. Buick *et al.* (2006) suggested an age for the Sandmata complex of 1720 Ma, which is in agreement with the age suggested by Bhowmik *et al.* (2010) (Proterozoic) who established the isotopic zircon metamorphic age of the Sandmata complex as 1700 Ma. The metamorphic age of the Mangalwar complex has been suggested as 970–930 Ma by Buick *et al.* (2010). Rocks of the BGC are overlain by regional Palaeo- to Mesoproterozoic sequences, termed the Aravalli Supergroup, which, in turn, are overlain by the youngest rocks of the region called the Delhi Supergroup, represented by Meso- to Neoproterozoic metasedimentary sequences which were deposited in the Delhi Basin that opened up at ~1.6 Ga and later closed at 0.9 Ga (Raja Rao, 1976; Gupta *et al.* 1980).

The Diwani hill granulites are part of the Aravalli–Delhi Mobile Belt situated in the Banaskantha district of Gujarat's northern part. Rock records of amphibolite and granulite facies, as well as certain obducted ophiolites, basement gneisses and blueschists are available in different parts of the Balaram Road area (Volpe & Macdougall, 1990; Tobisch *et al.* 1994; Biswal *et al.* 1998*a*,*b*; Srikarni *et al.* 2004; Bhowmik *et al.* 2010; Mukhopadhyay *et al.* 2010; Prakash *et al.* 2021). Charnockites, and a gabbro-norite-basic granulite suite, occur as shear zone bounded lensoidal bodies (Mahadani *et al.* 2015). Charnockites, basic granulites and gneisses are found as enclaves within granite gneiss. Different sets of fold axes (as F_1, F_2 and F_3 reported by Singh *et al.* 2010; Prakash

https://doi.org/10.1017/S0016756822000607 Published online by Cambridge University Press

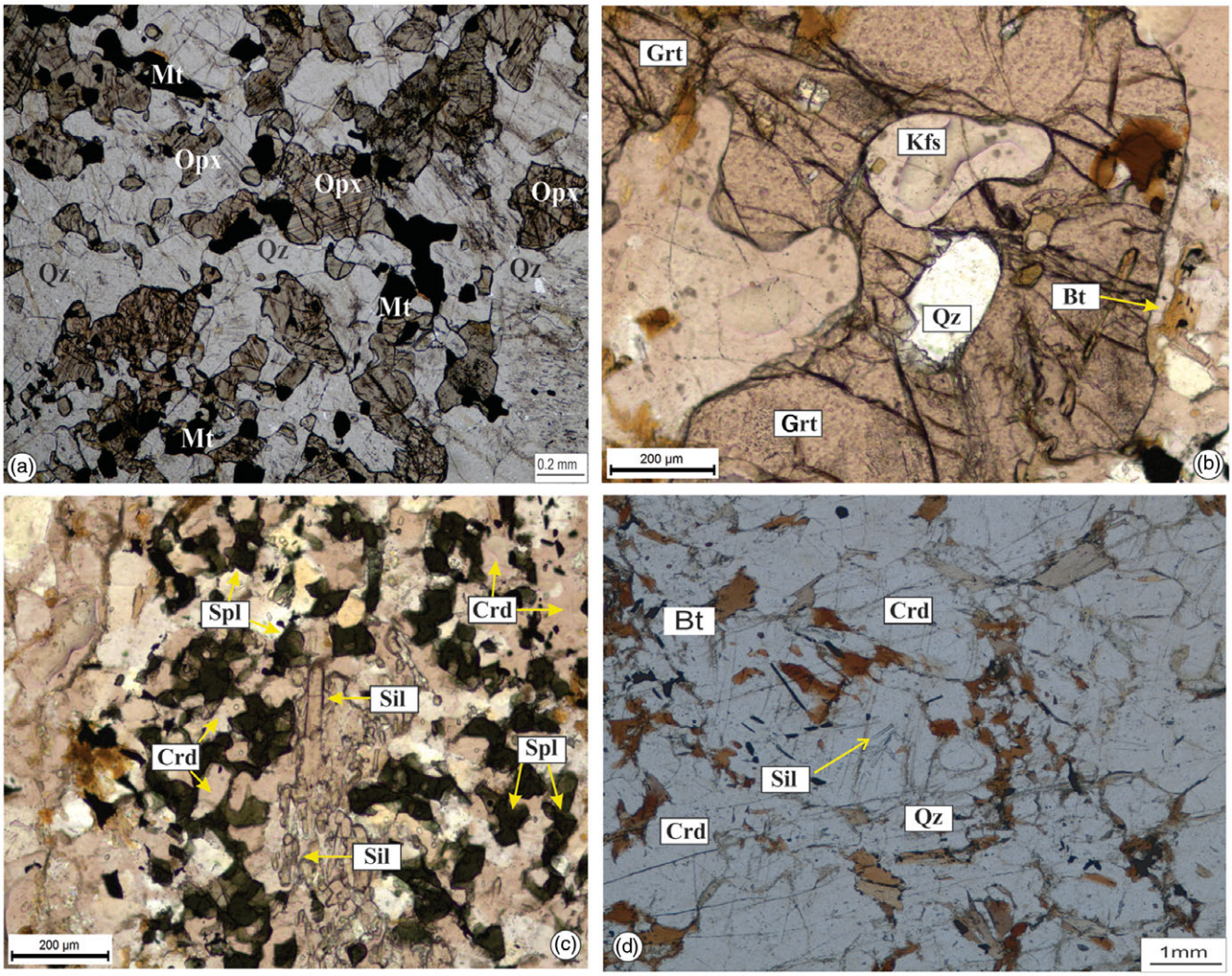

Fig. 2. (Colour online) (a) Photomicrographs showing co-existence of magnetite (Mt) with orthopyroxene (Opx) and quartz (Qz). (b) Photomicrographs showing garnet (Grt) with inclusions of quartz and alkali-feldspar (Kfs) (in plain polarized light, PPL). (c) Photomicrographs showing spinel (Spl) and cordierite (Crd) grains separated by sillimanite (Sil) (in PPL). (d) Biotite (Bt), sillimanite and quartz symplectite along with cordierite (in PPL).

et al. 2021) are present in the rocks of the Diwani hills, which suggests their conformable relationship with the regional-scale tectonic deformation in the Aravalli–Delhi Mobile Belt.

3. Oxidation condition and mineral chemistry

Pelitic granulites are dark in colour, medium (2–5 mm) to coarse (>5 mm) grained, and firm and compact. Despite the fact that foliation is not readily apparent at the macro level, microscopic analysis of biotite and orthopyroxene reveals a preferred orientation. The dominant mineral constituents of pelitic granulites are garnet, cordierite, K-feldspar, quartz, plagioclase, biotite, orthopyroxene and spinel. The textural features (Fig. 2a) of magnetite, orthopyroxene and quartz indicate an oxidation reaction during granulite metamorphism, which may be expressed in the balanced form as:

$$3\text{Ferrosilite} + O_2 \rightleftharpoons 2\text{Magnetite} + 6\text{Quartz} \quad (1)$$

The mineral compositions of typical rock types from the Diwani hills were analysed using the CAMECA SXFive electron probe microanalyser (EPMA) instrument coupled with SXFive software at the DST-SERB National Facility, Centre of Advanced Study in Geology, Institute of Science, Banaras Hindu University. The polished thin-sections were used for electron probe microanalysis using the LEICA-EM ACE200 apparatus for carbon coating. With a LaB6 source in the electron gun, electron beams were produced at an accelerating voltage of 15 kV and a beam current of 10 nA. For routine calibration, acquisition, quantification and data processing, CAMECA's SxSAB version 6.1 and SX-Results software were used. The precision of the analyses produced is better than 1 % for major-element oxides and 5 % for trace elements.

3.a. Garnet

Table 1 shows the electron microprobe data and structural formulae of garnet based on 12 oxygen atoms per formula unit (apfu) from the pelitic granulites. The X_{Mg} (= Mg/(Mg + Fe^{2+})) in the studied garnet grains ranges from 0.102 to 0.143. As seen in Figure 3a, the bulk of the garnets are solid solutions among the four end-members: almandine, pyrope, grossularite and spessartite. The composition data of the analysed garnets plotted on an Fe–

https://doi.org/10.1017/S0016756822000607 Published online by Cambridge University Press

Table 1. Representative electron microprobe analyses and structural formulae of garnet, spinel, cordierite and biotite

Sample no.	D/52	D/52	D/21	D/21	D/52	D/52	D/52	D/52	D/52	D/52	D/52	D/52	D/52	D/52	D/52	D/21
Spot no.	34	52	53	97	54	55	56	57	29	18	81	115	14	82	85	129
Mineral	**Grt**	**Grt**	**Grt**	**Grt**	**Spl**	**Spl**	**Spl**	**Spl**	**Crd**	**Crd**	**Crd**	**Crd**	**Bt**	**Bt**	**Bt**	**Bt**
SiO_2	36.70	37.20	36.25	37.02	0.18	0.12	0.21	0.20	47.69	48.67	48.62	48.90	35.36	36.20	35.37	35.78
TiO_2	0.02	0.03	0.04	0.03	0.02	0.00	0.02	0.00	0.00	0.00	0.00	0.00	3.37	3.94	4.71	4.19
Al_2O_3	20.34	20.45	20.15	20.44	56.78	56.61	55.67	54.97	31.84	31.94	31.17	39.09	17.13	15.67	15.40	15.66
Cr_2O_3	0.05	0.03	0.07	0.04	0.10	0.10	0.12	0.10	0.00	0.00	0.00	0.00	0.21	0.12	0.18	0.18
FeO	36.37	36.54	38.08	36.40	38.83	40.50	40.11	41.39	12.77	11.62	11.72	9.10	21.54	20.96	20.75	20.63
MnO	1.35	1.26	1.19	1.32	0.08	0.18	0.23	0.30	0.13	0.28	0.08	0.12	0.17	0.08	0.01	0.02
MgO	3.30	3.21	2.38	3.36	2.20	1.94	2.08	1.90	5.86	6.58	6.17	2.52	8.28	9.49	9.43	8.82
CaO	1.15	1.03	1.13	0.99	0.01	0.05	0.01	0.00	0.00	0.00	0.00	0.00	0.03	0.03	0.00	0.05
Na_2O	0.02	0.01	0.02	0.01	0.02	0.03	0.00	0.03	0.04	0.06	0.03	0.00	0.13	0.11	0.07	0.10
K_2O	0.03	0.03	0.08	0.02	0.02	0.02	0.02	0.02	0.00	0.00	0.00	0.00	9.51	9.47	9.44	9.56
Total	99.33	99.74	99.39	99.65	97.74	99.52	98.01	98.52	98.33	99.14	97.79	99.76	95.73	96.10	95.52	94.94
O basis	**12**	**12**	**12**	**12**	**4**	**4**	**4**	**4**	**18**	**18**	**18**	**18**	**22**	**22**	**22**	**22**
Si	2.992	3.014	2.980	3.003	0.005	0.003	0.006	0.006	5.013	5.046	5.104	4.933	5.438	5.527	5.451	5.528
Ti	0.001	0.002	0.002	0.002	0.000	0.000	0.000	0.000	0.000	0.000	0.000	0.000	0.390	0.452	0.546	0.487
Al	1.954	1.953	1.953	1.954	1.970	1.942	1.944	1.925	3.945	3.903	3.858	4.648	3.105	2.819	2.797	2.852
Cr	0.003	0.002	0.004	0.002	0.002	0.002	0.003	0.002	0.000	0.000	0.000	0.000	0.026	0.015	0.022	0.022
Fe^{2+}	2.430	2.443	2.558	2.431	0.922	0.934	0.935	0.949	10.80	0.956	0.992	0.768	2.770	2.676	2.674	2.665
Fe^{3+}	0.049	0.033	0.060	0.038	0.034	0.052	0.059	0.079	0.042	0.051	0.038	0.000	0.000	0.000	0.000	0.000
Mn	0.093	0.087	0.083	0.091	0.002	0.005	0.006	0.007	0.011	0.024	0.007	0.010	0.022	0.011	0.001	0.003
Mg	0.401	0.388	0.292	0.407	0.097	0.084	0.092	0.084	0.918	1.016	0.966	0.378	1.898	2.159	2.167	2.031
Ca	0.100	0.090	0.099	0.086	0.000	0.002	0.000	0.000	0.000	0.000	0.000	0.000	0.004	0.005	0.000	0.008
Na	0.004	0.002	0.004	0.001	0.001	0.001	0.000	0.002	0.009	0.011	0.005	0.000	0.038	0.033	0.022	0.030
K	0.003	0.003	0.009	0.002	0.001	0.001	0.001	0.001	0.000	0.000	0.000	0.000	1.866	1.845	1.855	1.884
X_{Mg}	**0.142**	**0.137**	**0.102**	**0.143**	**0.095**	**0.083**	**0.089**	**0.081**	**0.459**	**0.515**	**0.493**	**0.330**	**0.407**	**0.447**	**0.448**	**0.432**

$X_{Mg} = Mg/(Mg + Fe^{2+})$.

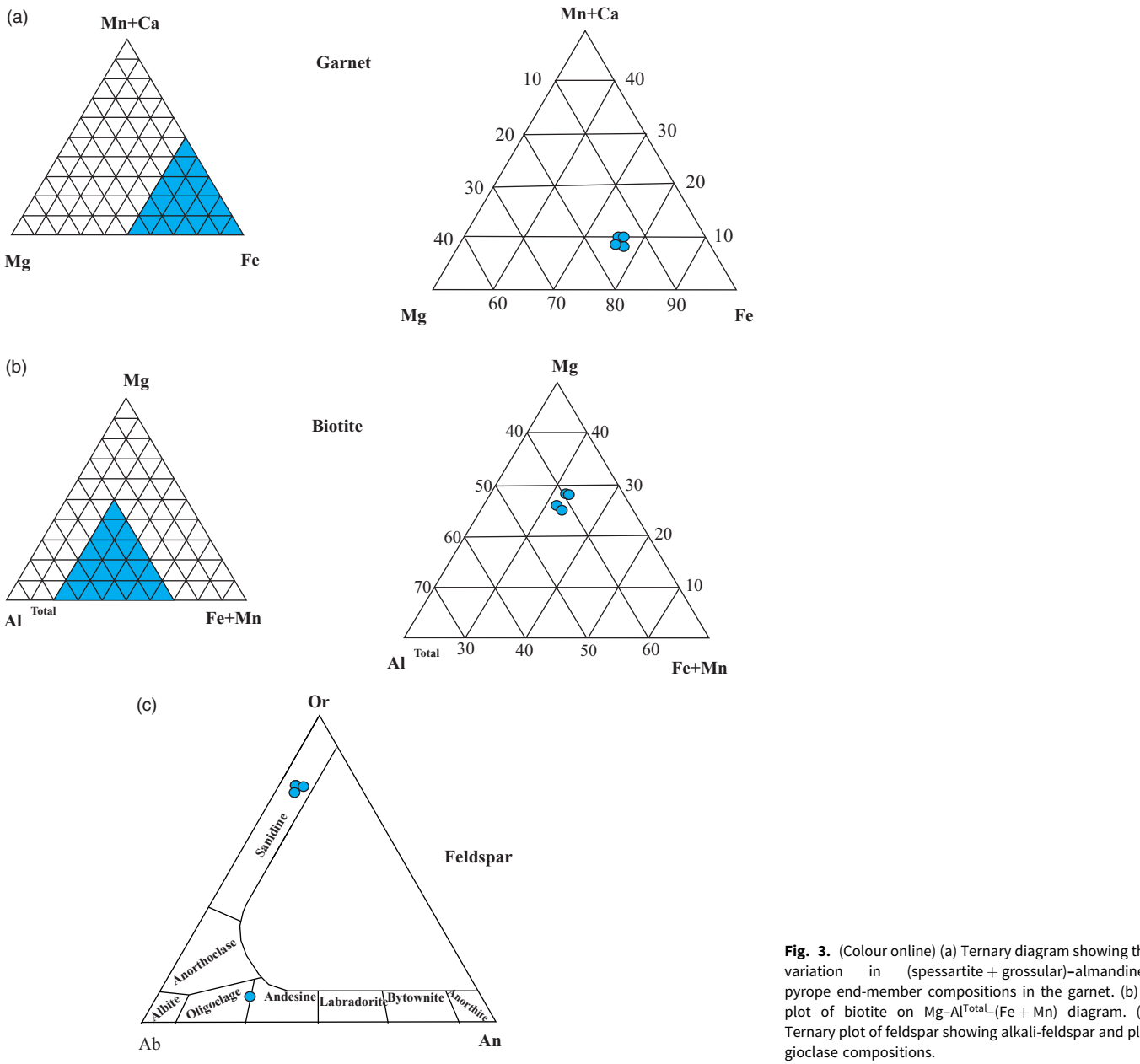

Fig. 3. (Colour online) (a) Ternary diagram showing the variation in (spessartite + grossular)–almandine–pyrope end-member compositions in the garnet. (b) A plot of biotite on Mg–Al^{Total}–(Fe + Mn) diagram. (c) Ternary plot of feldspar showing alkali-feldspar and plagioclase compositions.

Mg–(Ca + Mn) ternary diagram show a concentration in the almandine and pyrope regions (Fig. 3a). The garnets are relatively poor in manganese (0.083–0.093 apfu) and calcium (0.086 to 0.100 apfu).

3.b. Spinel

The investigated spinel is a solid solution of spinel (Mg) and hercynite (Fe^{2+}). Spinel found in the rock is mostly hercynite ($Fe^{2+}Al_2O_4$), with X_{Mg} values ranging from 0.081 to 0.095. Al_2O_3 (up to 56.78 wt %) and FeO (41.39 wt %) are both abundant in the spinel (Table 1).

3.c. Cordierite

The microprobe examinations of cordierite, on average, demonstrate low anhydrous sums of oxides, i.e. 97–99 % (Table 1), implying the existence of roughly 1–3 wt % of a hydrous component (H_2O and/or CO_2) retained inside structural channels. The X_{Mg} content of the cordierite varies from 0.330 to 0.515. Cordierite contains trace levels of sodium, potassium and to a lesser extent, calcium. Na_2O, K_2O and CaO are commonly found at concentrations of 0.03, 0.01 and 0.02 wt %, respectively.

3.d. Biotite

The structural formulae (based on 22 oxygen apfu) and microprobe investigations of biotite show a wide range of X_{Mg} values (Table 1), ranging from 0.407 to 0.448. The biotite has an Al concentration ranging from 2.797 to 3.105. The amount of Ti in the biotite ranges from 0.390 to 0.546. The concentration of TiO_2 is found to lie between 3.37 and 4.71 wt% in the biotite from the pelitic granulites of the studied area. Al content is more than that of Mg in the biotite, as shown in the ternary diagram (Fig. 3b).

https://doi.org/10.1017/S0016756822000607 Published online by Cambridge University Press

Table 2. Representative electron microprobe analyses and structural formulae of sillimanite, orthopyroxene, K-feldspar and ilmenite

Sample no.	D/52	D/52	D/52	D/52	D/21	D/21	D/21	D/52	D/52	D/52	D/21	D/21	D/21
Spot no.	122	123	125	126	112	113	12	111	112	130	23	46	63
Mineral	**Sil**	**Sil**	**Sil**	**Sil**	**Opx**	**Opx**	**Kfs**	**Kfs**	**Kfs**	**Kfs**	**Ilm**	**Ilm**	**Ilm**
SiO_2	37.71	37.31	41.15	37.40	48.01	47.91	66.06	64.80	65.15	65.49	0.00	0.00	0.14
TiO_2	0.00	0.04	0.00	0.07	0.05	0.04	0.00	0.00	0.00	0.00	53.10	52.91	51.49
Al_2O_3	62.07	61.69	56.35	61.72	7.91	8.10	18.36	18.03	18.27	18.45	0.00	0.00	0.00
Cr_2O_3	0.07	0.03	0.06	0.07	0.02	0.03	0.00	0.00	0.00	0.00	0.00	0.00	0.00
FeO	0.14	0.40	0.14	0.29	18.94	17.92	0.00	0.00	0.00	0.00	45.61	46.23	48.10
MnO	0.00	0.00	0.00	0.00	0.39	0.40	0.05	0.00	0.10	0.00	0.36	0.62	0.31
MgO	0.00	0.00	0.00	0.00	24.92	25.10	0.00	0.00	0.00	0.00	0.11	0.09	0.08
CaO	0.03	0.03	0.01	0.01	0.12	0.17	0.11	0.00	0.05	0.12	0.05	0.05	0.09
Na_2O	0.02	0.03	0.12	0.03	0.02	0.03	4.88	1.15	1.49	1.51	0.00	0.00	0.00
K_2O	0.00	0.04	1.80	0.01	0.12	0.14	9.49	14.82	14.39	14.18	0.00	0.00	0.00
Total	100.04	99.64	99.63	99.60	100.50	99.84	99.00	98.95	99.74	100.22	99.23	99.90	100.21
O basis	**5**	**5**	**5**	**5**	**6**	**6**	**8**	**8**	**8**	**8**	**6**	**6**	**6**
Si	1.627	1.620	1.795	1.623	1.760	1.760	3.011	3.013	3.006	3.007	0.000	0.000	0.007
Ti	0.000	0.001	0.000	0.002	0.000	0.000	0.000	0.000	0.000	0.000	2.032	2.011	1.985
Al	3.157	3.157	2.897	3.156	0.342	0.351	0.986	0.988	0.994	0.998	0.000	0.000	0.000
Cr	0.002	0.001	0.002	0.002	0.000	0.000	0.000	0.000	0.000	0.000	0.000	0.000	0.000
Fe^{2+}	0.005	0.015	0.005	0.011	0.581	0.551	0.000	0.000	0.000	0.000	1.941	1.953	1.968
Fe^{3+}	0.000	0.000	0.000	0.000	0.000	0.000	0.000	0.000	0.000	0.000	0.000	0.000	0.016
Mn	0.000	0.000	0.000	0.000	0.012	0.012	0.002	0.000	0.004	0.000	0.016	0.027	0.013
Mg	0.000	0.000	0.000	0.000	1.362	1.375	0.000	0.000	0.000	0.000	0.008	0.007	0.006
Ca	0.001	0.001	0.000	0.000	0.005	0.007	0.005	0.000	0.002	0.006	0.003	0.003	0.005
Na	0.002	0.003	0.010	0.003	0.000	0.000	0.431	0.104	0.133	0.134	0.000	0.000	0.000
K	0.000	0.002	0.099	0.001	0.006	0.007	0.552	0.879	0.847	0.831	0.000	0.000	0.000
X_{Mg}/X_K	0.000	0.000	0.000	0.000	0.701	0.714	0.558	0.895	0.862	0.855	0.000	0.000	0.000

$X_{Mg} = Mg/(Mg + Fe^{2+})$; $X_K = K/(K + Na + Ca)$.

3.e. Sillimanite

In the pelitic granulites, the Al_2SiO_5 polymorph sillimanite is found. Table 2 shows that the Al concentration ranges from 2.897 to 3.157. Ferric iron is the most common element that replaces aluminium in the sillimanite structure, but other elements viz. Ti, Cr, Ca, K, Na and Mn are also present in minor proportions.

3.f. Orthopyroxene

The Al_2O_3 content of the orthopyroxene in the pelitic granulites ranges from 7.91 to 8.10 wt %. The X_{Mg} in the orthopyroxenes shows variation (Table 2) from 0.701 to 0.714, and the Fe^{2+} content is as high as 0.581.

3.g. Feldspar

The structural formulae of the analysed plagioclase are identical to the ideal formula (Table 2). The ternary $NaAlSi_3O_8$–$KAlSi_3O_8$–$CaAl_2Si_2O_8$ diagram is used to map feldspars from the area (Fig. 3c). Cr, Ti, Fe, Mn and Mg are present in trace amounts. X_K values range from 0.558 to 0.895.

3.h. Ilmenite

Total Fe and Fe^{2+} have been measured in ilmenite. The absence of Fe^{3+} at the Ti-site or the presence of more than two divalent cations (based on six oxygens) indicate that Fe^{3+} is present in minor proportions (Table 2). FeO content in the sample goes up to 48.10 wt %.

4. Metamorphic conditions

In granulite-facies metamorphism, oxidation potential plays an important role in the stability and development of transition metal containing minerals, as well as limiting the occurrence and type of a C–O–H fluid phase (Newton, 1986; Lal *et al.* 1998).

In the present work, the pressure–temperature (*P*–*T*) and oxygen fugacity (log fO_2) conditions of the pelitic granulites were calculated simultaneously using Rob Berman's (2006) 'winTWQ'

https://doi.org/10.1017/S0016756822000607 Published online by Cambridge University Press

Table 3. Calculation of pressure–temperature and oxygen fugacity conditions at peak stage (sample no. D/52) by winTWQ program

Sample no.	Equilibria plotted in Fig. 4a	S(J/M)	V(J/BAR)
(a) The *P–T* condition obtained by specific equilibria for peak stage			
1	2 Py + 5 bQz + 4 Si = 3 Cd	108.20	15.53
2	2 Alm + 5 bQz + 4 Si = 3 fCd	135.73	16.30
3	3 fCd + 2 Py = 3 Cd + 2 Alm	−27.53	−0.78
Sample no.	**Equilibria plotted in Fig. 4b**	**S(J/M)**	V(J/BAR)
(b) The *T–f*O_2 condition obtained by specific equilibria for peak stage			
1	6 Fsl + O_2 = 2 Mt + 6 bQz	224.61	−3.35
2	3 Cd + 12 Fsl = 9 Qz + 2 Py + 4 Alm	−105.82	−19.44
3	4 Alm + 2 Py + 2 O_2 = 3 bQz + 4 Mt + 3 Cd	−343.41	26.15
4	6 Cd + 6 Fsl + 6 Mt = 4 Py + 8 Alm + 3 O_2	462.20	−48.96

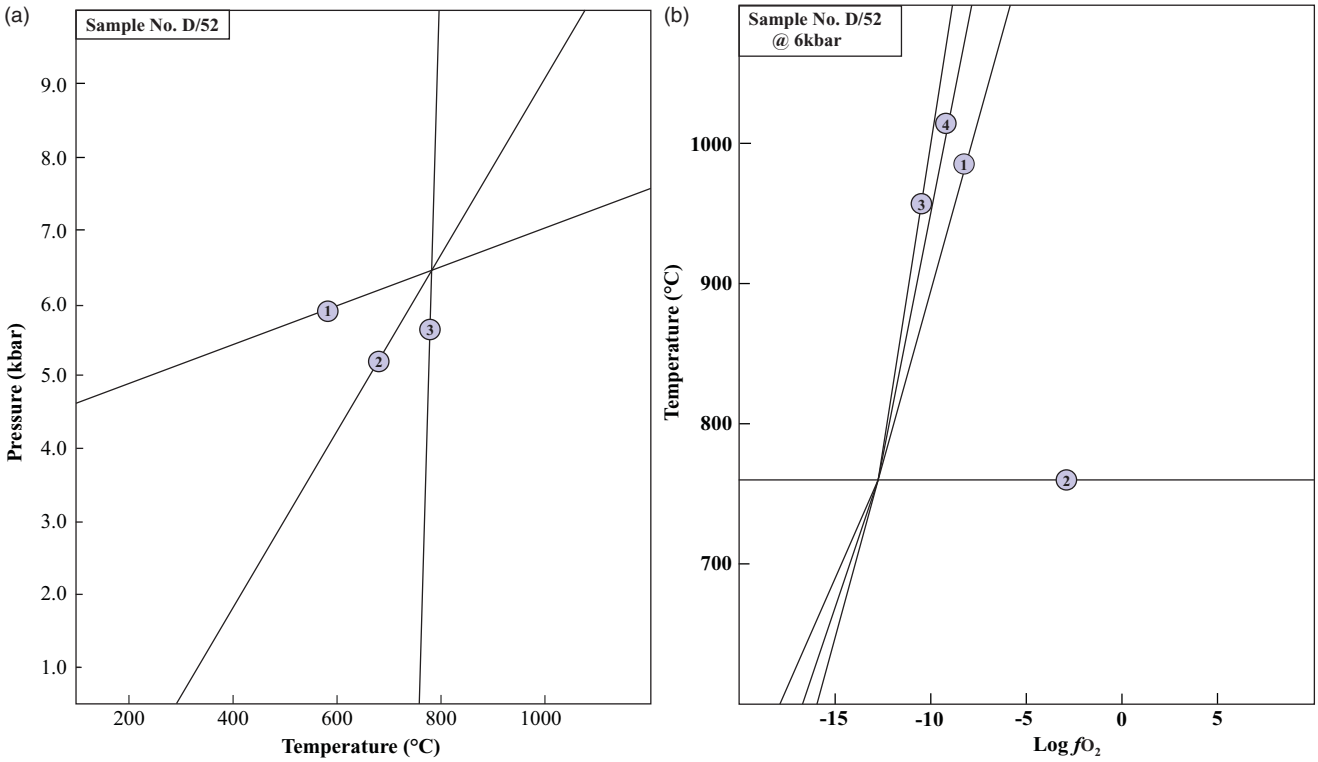

Fig. 4. (Colour online) (a) Results of the simultaneous calculations of pressure (*P*) and temperature (*T*) obtained using the winTWQ program with the intersection of specific equilibria for sample no. D/52 (data input from Tables 1, 2). (b) The intersection of specific equilibria for sample no. D/52 has been calculated simultaneously with the oxygen fugacity (fO_2) condition using the winTWQ tool (data input from Tables 1, 2).

computer program (version 2.32). *P–T* pseudosections relevant to the mineral assemblages preserved in these rocks are presented to constrain the peak metamorphic history of the pelitic granulites from the Diwani hills section. The location of reaction equilibria in *P–T* and oxygen fugacity (log fO_2) spaces is calculated using Berman & Aranovich's thermodynamic data (1996, updated December 2006) for the end-member phases. Almandine, pyrope, cordierite, sillimanite and beta-quartz are the end-member phases used in the winTWQ calculation for core compositions. For the selected end-member phases, three possible equilibria can be written (Table 3). The calculated *P–T* and (log fO_2) conditions for the pelitic granulites (sample no. D/52) are shown in Table 3 and Figure 4a, b. For the sample, the *P–T* obtained with the winTWQ program suggested near-thermal peak conditions of granulite-facies metamorphism of >770 °C at 7.6 kbar (Fig. 4a). At 6 kbar, the oxygen fugacity (log fO_2) versus temperature calculations yielded log fO_2 values of −13.0 and 770 °C, respectively (Fig. 4b).

The strong oxidation environment during granulite metamorphism in the area is indicated by the log fO_2 value (−13.0). According to the electron microprobe investigation, ilmenite in the sample includes limited Fe^{3+} concentration, i.e. 1–2 % of the haematite component, as assessed by charge balance considerations. Because of its sensitivity to changes in oxidation during

https://doi.org/10.1017/S0016756822000607 Published online by Cambridge University Press

Table 4. Solution notation, formulae and model sources for phase diagram calculation

Symbol in Perple_X solution model file	Symbol	Solution name	Formula	Source
Gt(HP)	Grt	Garnet	$Fe_{3x}Ca_{3y}Mg_{3z}Mn_{3(1-x-y-z)}$ $Al_2Si_3O_{12}$, $x+y+z \leq 1$	Holland & Powell (1998)
Opx(HP)	Opx	Orthopyroxene	$[Mg_xFe_{1-x}]_{2-y}Al_{2y}Si_{2-y}O_6$	Holland & Powell (1996)
Bio(TCC)	Bt	Biotite	$K[Mg_xFe_yMn_{1-x-y}]_{3-u-v-w}Fe^{3+}{}_wTi_uAl_{1+v}Si_{3-v}O_{10}(OH)_{2-2u}$, $x+y \leq 1$, $u+v+w \leq 1$	Tajcmanová *et al.* (2009)
hCrd	Crd	Cordierite	$Mg_{2x}Fe_{2y}Mn_{2(1-x-y)}$ $Al_4Si_5O_{18}\bullet(H_2O)_z$, $x+y \leq 1$	Ideal
Melt(HP)	melt	Melt	Na–Mg–Al–Si–K–Ca–Fe hydrous silicate melt	Holland & Powell (2001)
Kf	Kf	K-feldspar	$K_yNa_xCa_{1-x-y}Al_{2-x-y}Si_{2+x+y}O_8$, $x+y \leq 1$	Benisek *et al.* (2010)
Sp(GS)	sp	Spinel	$Mg_xFe_{1-x}Al_2O_3$	Ganguly & Saxena (1987)
Pl(JH)	Pl	Plagioclase	$K_yNa_xCa_{1-x-y}Al_{2-x-y}Si_{2+x+y}O_8$, $x+y \leq 1$	Jennings & Holland (2015)

Bulk composition in wt % is $Na_2O = 0.85$; $MgO = 3.73$; $MnO = 0.12$; $Al_2O_3 = 16.09$; $SiO_2 = 61.61$; $K_2O = 5.70$; $CaO = 0.19$; $TiO_2 = 1.13$; $FeO = 8.14$; $O_2 = 0.48$; $H_2O = 1.96$.

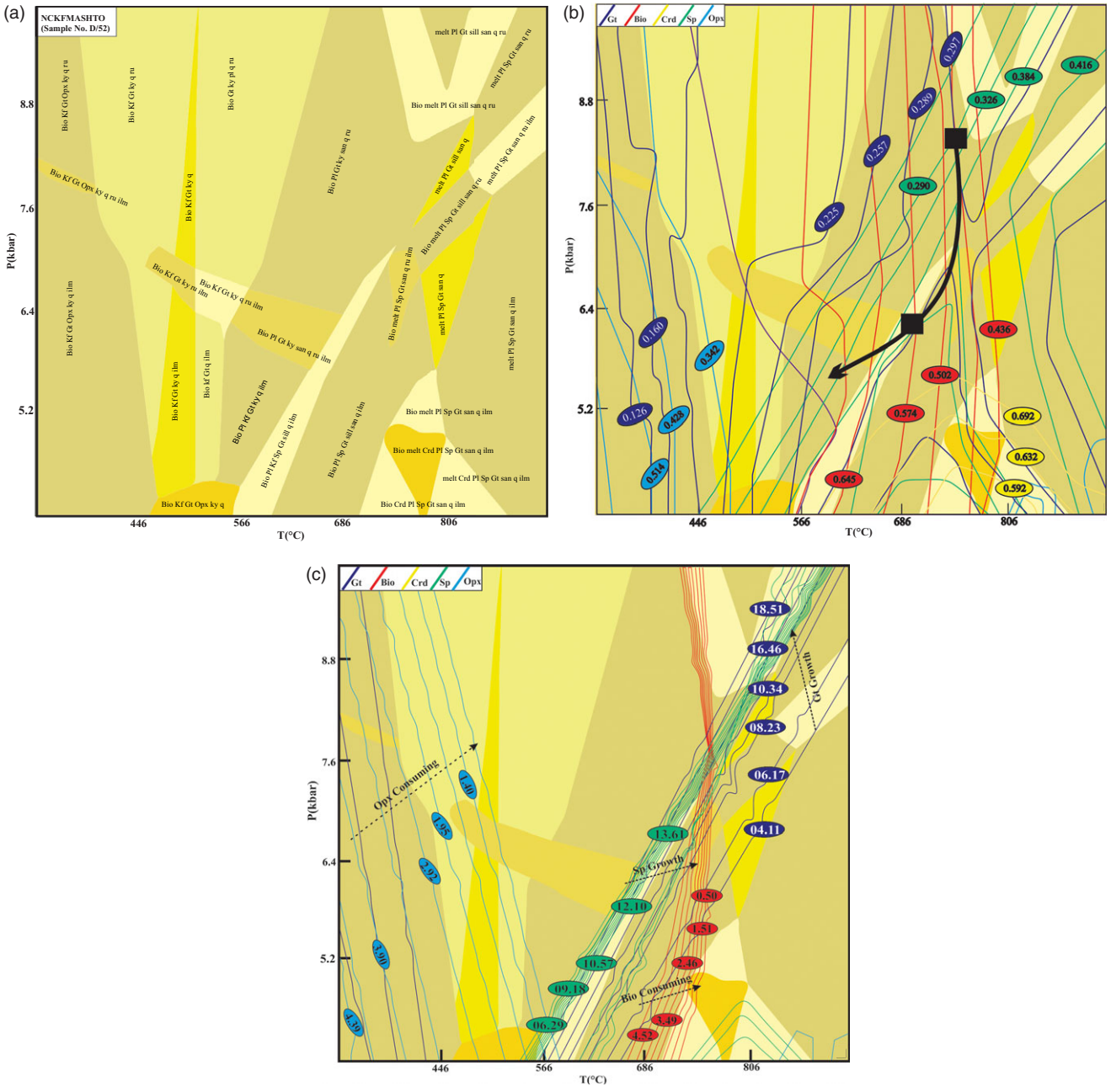

Fig. 5. (Colour online) (a) Calculated *P–T* pseudosection for the pelitic granulites (sample no. D/52) in the model system NCKFMASHTO (Na_2O–CaO–K_2O–FeO–MgO–MnO–Al_2O_3–SiO_2–H_2O–TiO_2–O_2). (b) Calculated *P–T* pseudosection for sample no. D/52 is contoured with calculated X_{Mg} (= Mg/(Mg + Fe^{2+})) isopleths of garnet, cordierite, orthopyroxene, spinel and biotite. (c) Distribution of the calculated modal isopleths of different minerals for the calculated pseudosection (sample no. D/52): garnet (Grt), biotite (Bt), spinel (Spl), cordierite (Crd) and orthopyroxene (Opx). Black dotted arrow represents growth and consumption of different minerals.

https://doi.org/10.1017/S0016756822000607 Published online by Cambridge University Press

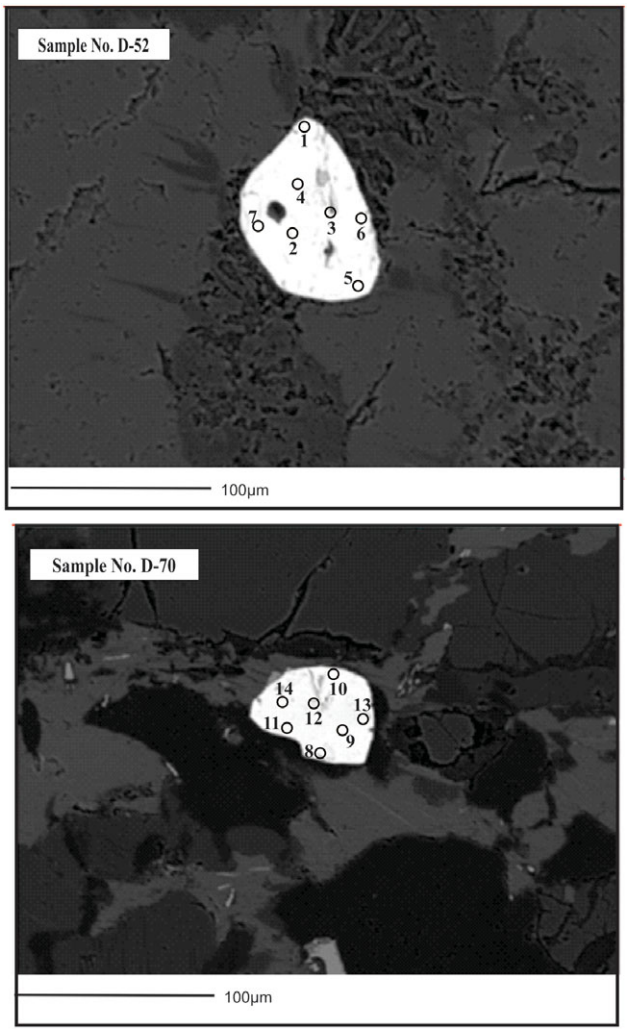

Fig. 6. Back-scattered electron (BSE) images of monazite grains (D/52 and D/70) from the Diwani hills.

metamorphism, graphite is commonly employed for log fO_2 measurement in granulite terranes. Graphite, on the other hand, is rare in the current area, which could be due to the strong oxidation conditions experienced during the metamorphism and subsequent exhumation of the Diwani hill granulites.

X-ray fluorescence (XRF) analyses of representative rock samples from the study area were performed on a Siemens SRS-3000 (WD-XRF) at the Wadia Institute of Himalayan Geology's X-ray Fluorescence Laboratory in Dehradun, India. The pseudosection depicts the various mineral assemblages in their respective stability fields derived from the specific bulk rock composition over a range of *P–T* conditions. The *P–T* pseudosection was built using the Perple_X program (version 6.8.7), which is based on Gibbs free energy minimization (Connolly & Petrini, 2002; Connolly, 2009). The pseudosections were constructed with the help of an internally consistent thermodynamic dataset and the equation of state for H_2O from Holland & Powell (1998). Table 4 contains the solution models' precise formulae, notation and sources. Mineral abbreviations used in this work are after Kretz (1983). To constrain the history of the pelitic granulites of the studied area, *P–T* pseudosections relevant to the mineral assemblages preserved in these rocks have been presented in Figure 5a. The pseudosection for the pelitic granulites (sample no. D/52) is contoured with the compositional isopleths of X_{Mg} garnet, X_{Mg} biotite, X_{Mg} cordierite, X_{Mg} orthopyroxene and X_{Mg} spinel (Fig. 5b). The *P–T* conditions derived from the intersection of X_{Mg} isopleths of garnet, biotite and spinel give a peak temperature of ~770 °C at 8.6 kbar.

5. Monazite geochronology

The EPMA monazite geochronology was used to determine the age and evolutionary history of the southern section (Diwani hills) of the Aravalli–Delhi Mobile Belt. Electron microprobe dating can be a very useful instrument for determining the age of metamorphism and deformation history of a rock. After systematic electron microprobe – backscatter electron (EPMA–BSE) imaging, two samples (D/52 and D/70) were selected for microprobe dating that had grain sizes ranging from 83 to 115 microns and a uniform mineral composition (Fig. 6). In the BSE images, the monazite grains exhibit uniform compositional domains. Monazite grains range in shape from anhedral to subhedral or rounded, and in size from small (30–80 µm) to large (80–115 µm). They can be found as an inclusion within garnet and as the matrix. In the present study, monazite grains occur as inclusions in garnet porphyroblasts and have a lower yttrium (Y) elemental composition at the rim than the core. The partitioning of Y in monazite is directly related to the growth or consumption of peritectic garnet (Spear & Pyle, 2010; Bhowmik *et al.* 2014). The monazite exhibits compositional variation between Th (Ca and Si) and Y (heavy rare earth elements), and it reflects the various substitutions. The SiO_2 content of all the monazite grains seemed to be negligible.

The isotopic data (Fig. 7a; Table 5) of the monazite grains have been interpreted to date the metamorphic event in the Diwani hills as Neoproterozoic (817 ± 19 Ma). Figure 7b shows the probability density peaks of monazite ages from different samples, as well as a probability density plot of spot dates with a single peak at ~810 Ma.

The results of the monazite geochronology in this study provide the current understanding that the enclave granulite-facies domain in the Balaram area is the result of a widespread Neoproterozoic (817 ± 19 Ma) tectonothermal event.

6. Discussion

Based on the petrographic analysis, mineralogical criteria, oxygen fugacity, pseudosection modelling and geochronological data, an attempt was made to determine the tectonometamorphic evolution of the Diwani hill area. The calculated metamorphic *P–T* conditions clearly show that the investigated area followed an isothermal decompressional path (with a pressure change of ~2.4 kbar). Graphite, one of the most oxidation sensitive minerals, is very common in the granulites of southern India. However, graphite is typically absent in the studied rock samples of the current area, which could be attributed to the high-oxidation conditions (log fO_2 up to −13) during metamorphism and subsequent exhumation of the granulite of the Diwani hills. The granulites in the study area lack any exsolution textures and corona textures, so there lies a possibility of high CO_2 flux catalysing retrograde reactions, in the absence of which these inequilibrium textures could else have been preserved. CO_2 is the only volatile that could be abundant enough to dilute and carry off H_2O sufficiently to consume hydrous phases, and evidence of high oxygen fugacities also suggests that there could be a high-pressure CO_2-rich phase during

https://doi.org/10.1017/S0016756822000607 Published online by Cambridge University Press

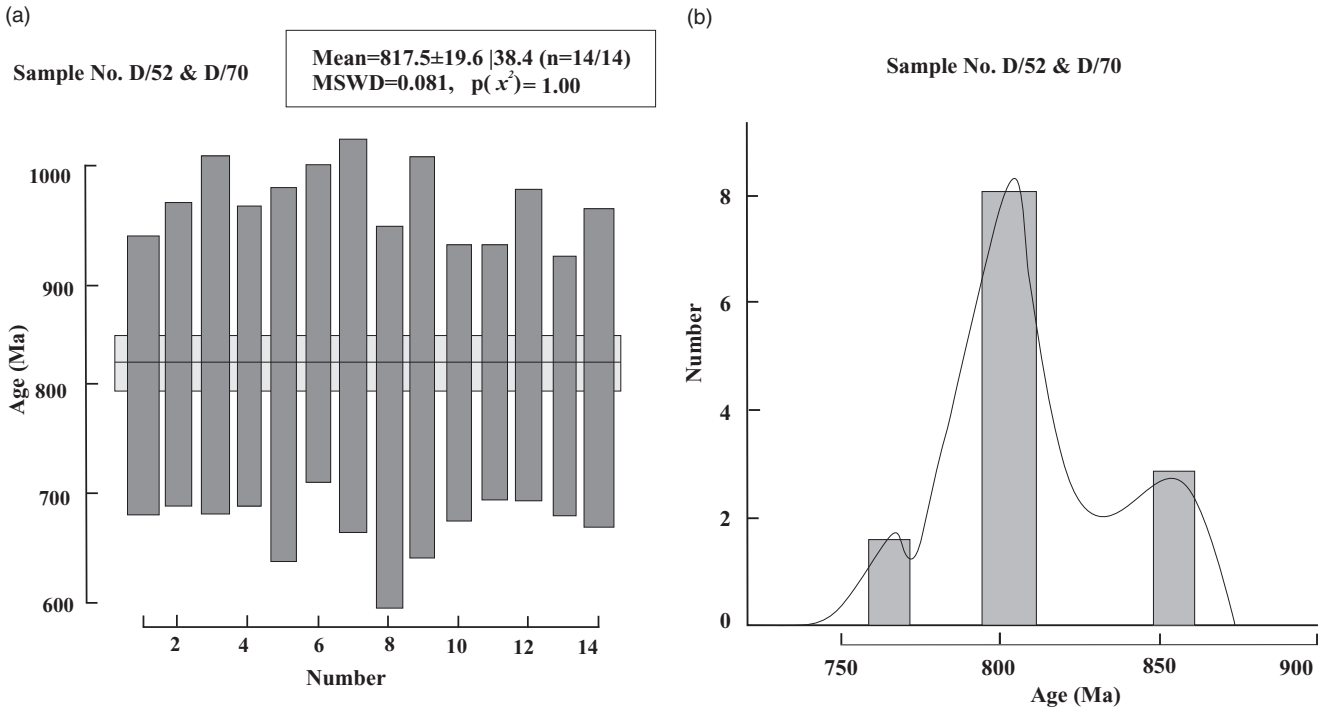

Fig. 7. (a) The weighted average of mean ages from monazite in the sample (D/52 and D/70). (b) A probability density plot of spot dates reveals a single peak at ~817 Ma.

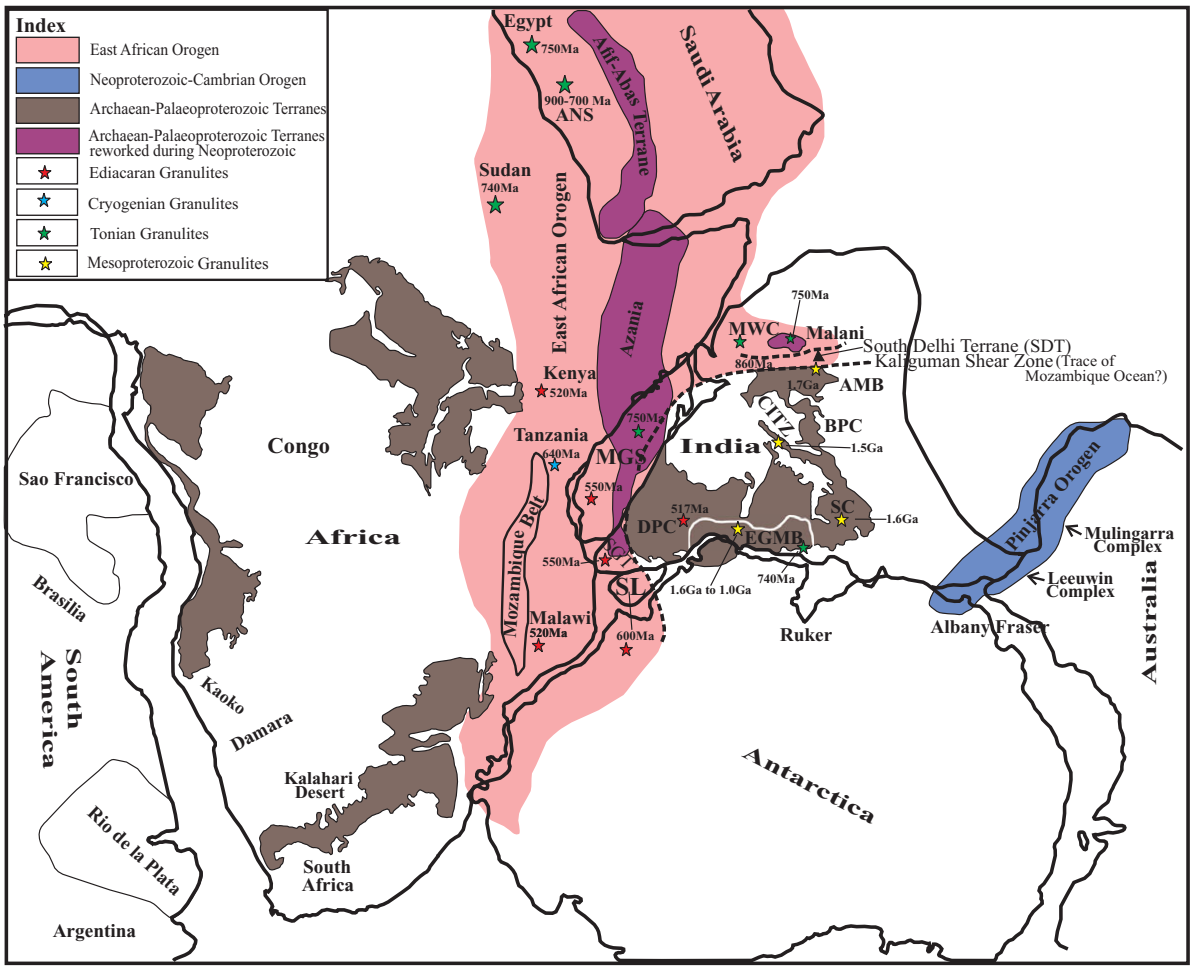

Fig. 8. (Colour online) Reconstruction of part of Gondwana showing various cratonic blocks modified after Prakash *et al*. (2021). ANS – Arabian Nubian Shield; AMB – Aravalli Mobile Belt; BPC – Bundelkhand Protocontinent; CITZ – Central India Tectonic Zone; DPC – Dharwar Protocontinent; EGMB – Eastern Ghats Mobile Belt; MGS – Madagascar; MWC – Marwar Craton; SC – Singhbhum Craton; SGT – Southern Granulite Terrane; SL – Sri Lanka.

https://doi.org/10.1017/S0016756822000607 Published online by Cambridge University Press

Table 5. EPMA dating age of monazite crystals of pelitic granulites (sample no. D/52 and D/70)

Points	Al_2O_3	SiO_2	P_2O_5	CaO	Y_2O_3	La_2O_3	Ce_2O_3	Pr_2O_3	Nd_2O_3	Sm_2O_3	Eu_2O_3	PbO	UO_2	ThO_2	Total	Age (Ma)	±2σ
D/52 Mnz-01	−0.008	0.088	30.234	1.521	1.143	13.121	27.649	4.324	11.419	2.004	0.153	0.341	0.786	7.216	100.00	808	65
D/52 Mnz-02	0.031	0.401	30.946	1.505	0.335	13.557	27.721	4.407	11.968	2.281	0.084	0.318	0.685	6.652	100.89	828	71
D/52 Mnz-03	−0.008	0.239	31.243	1.446	0.240	13.899	28.517	4.321	11.981	2.272	0.021	0.272	0.450	5.996	100.89	846	84
D/52 Mnz-04	0.017	0.279	29.376	1.522	0.202	13.594	28.495	4.321	11.907	2.162	0.041	0.325	0.588	7.188	100.02	826	70
D/52 Mnz-05	0.013	0.424	31.192	1.348	0.159	13.803	28.634	4.431	12.300	2.349	0.068	0.248	0.456	5.630	101.05	808	87
D/52 Mnz-06	−0.014	0.209	30.618	1.527	0.238	13.669	28.086	4.387	12.473	2.274	0.088	0.315	0.600	6.571	101.05	855	75
D/52 Mnz-07	−0.008	0.228	31.071	1.188	0.118	14.190	29.325	4.587	12.399	2.272	0.059	0.244	0.467	5.164	101.31	843	92
D/70 Mnz-08	0.014	0.435	29.436	1.352	0.719	13.119	28.475	4.452	12.253	2.106	−0.006	0.233	0.151	6.579	99.33	769	89
D/70 Mnz-09	−0.008	0.172	31.427	1.470	0.650	13.300	28.246	4.476	12.161	2.057	−0.046	0.240	0.285	5.826	100.31	824	93
D/70 Mnz-10	−0.007	0.255	30.127	1.460	0.465	13.210	27.404	4.391	11.730	2.057	-0.054	0.345	0.959	6.825	99.23	801	65
D/70 Mnz-11	0.020	0.358	29.566	1.583	0.572	12.780	26.807	4.105	11.656	2.076	0.002	0.376	1.297	6.449	97.65	812	60
D/70 Mnz-12	0.008	0.253	29.750	1.474	0.511	13.101	27.517	4.306	12.031	2.116	−0.054	0.313	0.709	6.378	98.47	833	73
D/70 Mnz-13	−0.007	0.586	29.746	1.398	0.613	13.028	27.369	4.382	11.708	2.000	0.145	0.361	1.328	6.127	98.79	797	61
D/70 Mnz-14	0.003	0.190	29.660	1.346	0.504	13.490	28.387	4.473	12.222	2.189	−0.028	0.294	0.805	5.736	99.30	814	75

metamorphism (Newton, 1986). Although some previous workers have attempted to determine the isotopic age of the rocks of the Diwani hill region, controversy over the age of these granulites still exists. According to Singh *et al.* (2010), metamorphism of the Diwani hill granulites took place between *c.* 860 and 800 Ma, while exhumation through thrusting along multiple ductile shear zones took place at *c.* 800–760 Ma. Biju-Sekhar *et al.* (2003) used electron microprobe dating of monazite and zircon in granites and estimated a 1.8–1.7 Ga Palaeoproterozoic magmatic event in the Aravalli–Delhi Mobile Belt.

Previous work, based on SHRIMP U–Pb chronological studies, yielded ages corresponding to a metamorphic overprint between 780 and 680 Ma, and ages corresponding to detritus derived from a magmatic source between 1591 and 1216 Ma (Singh *et al.* 2010; Prakash *et al.* 2021). However, in the present study, we only obtained a metamorphic overprint date (769 to 855 Ma).

Around 800 Ma or a little earlier, as evident by the magmatism and metamorphic history, the existence of the proposed Malani supercontinent consisted of India, the Arabian Nubian Shield (ANS), Madagascar and China (Kochhar, 2008). It has been inferred that the present NW India was adjacent to the East African Orogen on its eastern margin (Vijaya *et al.* 2000). The South Delhi Terrane (SDT) is the part of NW India (Fig. 8).

The SDT is regarded as a suture zone between the western component of Gondwana (including East Africa, Madagascar and the ANS, and oceanic arcs such as the Bemarivo Belt of northern Madagascar and the Seychelles) and the eastern component of Gondwana (including the Dharwar–Marwar Craton and the Aravalli Mobile Belt – Bundelkhand Protocontinent). The SDT is characterized by multiple phases of folding episodes, high-grade metamorphism and a related orogeny between 1.7 Ga and 0.8 Ga (Choudhary *et al.* 1984; Volpe & Macdougall, 1990; Tobisch *et al.* 1994; Deb *et al.* 2001). This has been marked as a suture zone owing to similarity in the terrane components (Prakash *et al.* 2021 and references therein). On the basis of existing evidence, it has been suggested that the South Delhi basin may represent a remnant of the proto-Mozambique Ocean in NW India which was closed during subduction. As a result of this subduction, sediments metamorphosed to granulite-facies and were exhumed via thrusting during Neoproterozoic times.

As the Diwani hills represent part of the Aravalli–Delhi Mobile Belt, the present study attempted to determine the age and evolutionary history of the metamorphism of the Diwani hill granulites of the Aravalli–Delhi Mobile Belt with the help of the EPMA monazite (present as an inclusion within garnet and as the matrix in pelitic rocks) geochronology. In accordance with Singh *et al.* (2010) and Prakash *et al.* (2021), there existed a palaeo-subduction zone known as the Kaliguman Shear Zone (which demarcates the boundary suture between the SDT and the Aravalli–Bhilwara terrane) in the Aravalli–Delhi Mobile Belt along which the South Delhi basin might have been closed (Sugden *et al.* 1990; Biswal *et al.* 1998*a*). Based on the interpretation of the monazite geochronology, the present study infers that a metamorphic event occurred in the Diwani hill area at ~817 ± 19 Ma due to subduction. This finding further strengthens the previous model (Singh *et al.* 2010; Prakash *et al.* 2021) which argued that a subduction-related compressional tectonic regime might have been responsible for granulite-facies metamorphism of rocks in the Diwani hill area.

https://doi.org/10.1017/S0016756822000607 Published online by Cambridge University Press

7. Conclusions

The pelitic granulites from the Balaram area follow a clockwise *P–T* path of metamorphic evolution with 2.4 kbar of decompression, linked to simultaneous subduction and/or collisional tectonic processes. The calculated high-oxidation conditions for peak stages, as well as the absence of exsolution textures and spinel trellis textures, indicate that the granulite-facies metamorphism was highly CO_2 fluxed. The absence of graphite in the pelitic granulites is due to high log fO_2 values. The geochronological study of monazite grains demonstrates a metamorphic age of the Diwani hill granulites as Neoproterozoic (817 ± 19 Ma).

Acknowledgements. We extend our thanks to DST-SERB research project (P-07/704) to D.P. and JRF (CSIR) to M. Kumar for the financial help in the form of a fellowship. The authors thank anonymous reviewers for constructive comments that led to substantial improvements to the manuscript.

References

Benisek A, Dachs E and Kroll H (2010) A ternary feldspar-mixing model based on calorimetric data: development and application. *Contributions to Mineralogy and Petrology* **160**, 327–37.

Berman RG (2006) *winTWQ (version 2.3): A Software Package for Performing Internally-Consistent Thermobarometric Calculations*. Geological Survey of Canada, Open File 5462, 41 pp.

Berman RG and Aranovich LY (1996) Optimized standard state and solution properties of minerals. *Contributions to Mineralogy and Petrology* **126**, 1–24.

Bhowmik SK, Bernhardt HJ and Dasgupta S (2010) Grenvillian age high-pressure upper amphibolite-granulite metamorphism in the Aravalli-Delhi Mobile Belt, Northwestern India: new evidence from monazite chemical age and its implication. *Precambrian Research* **178**, 168–84.

Bhowmik SK, Wilde SA, Bhandari A and Basu Sarbadhikari A (2014) Zoned monazite and zircon as monitors for the thermal history of granulite terranes: an example from the Central Indian Tectonic Zone. *Journal of Petrology* **55**, 585–621.

Biju-Sekhar S, Yokoyama K, Pandit MK, Okudaira T, Yoshida M and Santosh M (2003) Late Paleo-Proterozoic magmatism in Delhi Fold Belt, NW India and its implication: evidence from EPMA chemical ages of zircons. *Journal of Asian Earth Sciences* **22**, 189–207.

Biswal TK, Gyani KC, Parthasarathy R and Pant DR (1998a) Tectonic implication of geochemistry of gabbronorite-basic granulite suite in the Proterozoic Delhi Supergroup, Rajasthan, India. *Journal of the Geological Society of India* **52**, 721–32.

Biswal TK, Gyani KC, Parthasarathy R and Pant DR (1998b) Implications of the geochemistry of the pelitic granulites of the Delhi Supergroup, Aravalli Mountain Belt, Northwestern India. *Precambrian Research* **87**, 75–85.

Buick IS, Allen C, Pandit M, Rubatto D and Hermann J (2006) The Proterozoic magmatic and metamorphic history of the Banded Gneissic Complex, central Rajasthan, India: LA-ICP-MS U–Pb zircon constraints. *Precambrian Research* **15**, 119–42.

Buick IS, Clark C, Rubatto D, Hermann J, Pandit M and Hand M (2010) Constraints on the Proterozoic evolution of the Aravalli–Delhi Orogenic belt (NW India) from monazite geochronology and mineral trace element geochemistry. *Lithos* **120**, 511–28.

Cho M, Kim Y and Ahn J (2007) Metamorphic evolution of the Imjingang belt, Korea: implications for Permo-Triassic collisional orogeny. *International Geological Review* **49**, 30–51.

Choudhary AK, Gopalan K and Sastry CA (1984) Present status of the geochronology of the Precambrian rocks of Rajasthan. *Tectonophysics* **105**, 131–40.

Connolly JAD (2009) The geodynamic equation of state: what and how. *Geochemistry, Geophysics, Geosystems* **10**, Q10014. doi: 10.1029/2009GC002540.

Connolly JAD and Petrini K (2002) An automated strategy for calculation of phase diagram sections and retrieval of rock properties as a function of physical conditions. *Journal of Metamorphic Geology* **20**, 697–708.

Deb M, Thorpe RI, Krstic D, Corfu F and Davis DW (2001) Zircon U–Pb and galena Pb isotope evidence for an approximate 1.0 Ga terrane constituting the western margin of the Aravalli-Delhi orogenic belt, northwestern India. *Precambrian Research* **10**, 8195–213.

Desai SJ, Patel MP and Merh SS (1978) Polymetamorphites of Balaram-Abu Road Area North Gujarat and Southwest Rajasthan. *Journal of the Geological Society of India* **19**, 383–94.

D'Souza J, Prabhakar N, Sheth H and Xu Y (2021) Metamorphic *P–T–t–d* evolution of the Mesoproterozoic Pur-Banera supracrustal belt, Aravalli Craton, northwestern India: insights from phase equilibria modelling and zircon–monazite geochronology of metapelites. *Journal of Metamorphic Geology* **39**, 1173–204.

D'Souza J, Prabhakar N, Xu Y, Sharma KK and Sheth H (2019) Mesoarchaean to Neoproterozoic (3.2–0.8 Ga) crustal growth and reworking in the Aravalli Craton, northwestern India: insights from the Pur-Banera supracrustal belt. *Precambrian Research* **332**, 105383. doi: 10.1016/j.precamres.2019.105383.

Ganguly J and Saxena S (1987) Mixtures and mineral reactions. In *Minerals and Rocks, Vol. 19* (A El Goresy, W Von Engelhardt and T Hahn), pp. 1–291. Berlin: Springer-Verlag.

Gomez-Rivas E, Butler RW, Healy D and Alsop I (2020) From hot to cold – the temperature dependence on rock deformation processes: an introduction. *Journal of Structural Geology* **132**, 103977. doi: 10.1016/j.jsg.2020.103977.

Gupta BC (1934) The geology of the central Mewar. Memoirs of the Geological Survey of India 65, 107–69.

Gupta SN, Arora YK, Mathur RK, Iqbaluddin BP, Sahai TN, Sharma SB and Murthy MVN (1980) *Lithostratigraphic Map of Aravalli Region, Southern Rajasthan and Northeastern Gujarat*. Hyderabad: Geological Survey of India.

Hazarika P, Upadhyay D and Mishra B (2013) Contrasting geochronological evolution of the Rajpura-Dariba and Rampura-Agucha metamorphosed Zn-Pb deposit, Aravalli-Delhi Belt, India. *Journal of Asian Earth Sciences* **73**, 429–39.

Heron AM (1953) Geology of central Rajasthan. *Memoirs of the Geological Survey of India* **79**, 1–389.

Holland T and Powell R (1996) Thermodynamics of order-disorder in minerals: I. Symmetric formalism applied to minerals of fixed composition. *American Mineralogist* **81**, 1413–24.

Holland TJB and Powell R (1998) An internally consistent thermodynamic data set for phases of petrological interest. *Journal of Metamorphic Geology* **16**, 309–43.

Holland T and Powell R (2001) Calculation of phase relations involving haplogranitic melts using an internally consistent thermodynamic dataset. *Journal of Petrology* **42**, 673–83.

Jennings ES and Holland TJ (2015) A simple thermodynamic model for melting of peridotite in the system NCFMASOCr. *Journal of Petrology* **56**, 869–92.

Kochhar N (2008) A-type Malani magmatism: signatures of the Pan-African Event in the NW Indian shield and assembly of the late Proterozoic Malani Supercontinent. *Geological Survey of India Special Publication* **91**, 112–28.

Kretz R (1983) Symbols for rock-forming minerals. *American Mineralogist* **68**, 277–9.

Lal SN, Thomas H and Prakash D (1998) Oxidation condition during granulite metamorphism in Anakapalle area, Eastern Ghats belt, India. *Proceedings of the National Academy of Sciences India* **68**, 181–4.

Mahadani T, Biswal TK and Mukherjee T (2015) Strain estimation of folds, orbiculites and quartz phenocrysts in the Ambaji Basin of the South Delhi Terrane, Aravalli-Delhi Mobile Belt, NW India and its tectonic implication. *Journal of the Geological Society of India* **85**, 139–52.

Mukhopadhyay D, Chattopadhyay N and Bhattacharyya T (2010) Structural evolution of a gneiss dome in the axial zone of the Proterozoic South Delhi Fold Belt in Central Rajasthan. *Journal of the Geological Society of India* **75**, 18–31.

Naqvi SM and Rogers JJW (1987) *Precambrian Geology of India*. New York: Oxford University Press.

Newton RC (1986) Fluids of granulite-facies metamorphism. In *Fluid–Rock Interactions during Metamorphism* (eds JV Walther and BJ Wood), pp. 36–59. New York: Springer.

Prakash D, Kumar M, Rai SK, Singh CK, Singh S, Yadav R, Jaiswal S, Srivastava V, Yadav MK, Bhattacharjee S and Singh PK (2021) Metamorphic P–T evolution of Hercynite-quartz-bearing granulites from the Diwani hills, North East Gujarat (NW India). *Precambrian Research* **352**, 105997. doi: 10.1016/j.precamres.2020.105997.

Raja Rao CS (1976) Precambrian sequences of Rajasthan. *Miscellaneous Publications of the Geological Survey of India* **23**, 497–516.

Roy AB and Kröner A (1996) Single zircon evaporation ages constraining the growth of the Archaean Aravalli craton, northwestern Indian shield. *Geological Magazine* **133**, 333–42.

Schulz B (1990) Prograde–retrograde *P–T–t*-deformation path of Austroalpine mica-schists during Variscan continental collision (Eastern Alps). *Journal of Metamorphic Geology* **8**, 629–43.

Singh YK, De WB, Karmakar S, Sarkar S and Biswal TK (2010) Tectonic setting of the Balaram-Kui-Surpagla-Kengora granulites of the South Delhi Terrane of the Aravalli Mobile Belt, NW India and its implication on correlation with the East African Orogen in the Gondwana assembly. *Precambrian Research* **183**, 669–88.

Sinha-Roy S, Malhotra G and Guha DB (1995) A transect across Rajasthan Precambrian terrain in relation to geology, tectonics and crustal evolution of south-central Rajasthan. In *Continental Crust of NW and Central India* (eds S Sinha-Roy and KR Gupta), pp. 63–90. Memoirs of the Geological Survey of India vol. 31.

Spear FS and Pyle JM (2010) Theoretical modeling of monazite growth in a low-Ca metapelite. *Chemical Geology* **273**, 111–19.

Srikarni C, Limaye MA and Janardhan AS (2004) Saphirine bearing granulites from Abu-Balaram area, Gujarat State: implications for India-Madagascar Connection. *Gondwana Research* **7**, 1214–18.

St-Onge MR, Rayner N, Palin RM, Searle MP and Waters DJ (2013) Integrated pressure-temperature-time constraints for the Tso Morari dome (Northwest India): implication for the burial and exhumation path of UHP units in the western Himalaya. *Journal of Metamorphic Geology* **31**, 469–504.

Sugden TJ, Deb M and Windley BF (1990) The tectonic setting of mineralisation in the Proterozoic Aravalli-Delhi orogenic belt, NW India. In *Precambrian Continental Crust and Its Economic Resources* (ed. SM Naqvi), pp. 367–90. New York: Elsevier.

Tajcmanová L, Connolly J and Cesare B (2009) A thermodynamic model for titanium and ferric iron solution in biotite. *Journal of Metamorphic Geology* **27**, 153–64.

Tobisch OT, Collerson KD, Bhattacharya T and Mukhopadhyay D (1994) Structural relationship and Sm–Nd isotope systematics of polymetamorphic granitic gneisses and granitic rocks from central Rajasthan, India – implications for the evolution of the Aravalli craton. *Precambrian Research* **65**, 319–39.

Triboulet C and Audren C (1985) Continuous reactions between biotite, garnet, staurolite, kyanite-sillimanite-andalusite and P-T-time-deformation path in micaschists from the estuary of the river Vilaine, South Brittany, France. *Journal of Metamorphic Geology* **3**, 91–105.

Valdiya KS (2010) Some burning questions remaining unanswered. *Journal of the Geological Society of India* **78**, 299. doi: 10.1007/s12594-011-0097-1.

Vijaya RV, Prasad RB, Reddy PR and Tewari HC (2000) Evolution of Proterozoic Aravalli Delhi Fold Belt in the north western Indian Shield from seismic studies. *Tectonophysics* **327**, 109–30.

Volpe AM and Macdougall JD (1990) Geochemistry and isotopic characteristics of mafic (Phulad Ophiolite) and related rocks in the Delhi Supergroup, Rajasthan, India: implications for rifting in the Proterozoic. *Precambrian Research* **48**, 167–91.